Aerosol Science and Technology

ISSN: 0278-6826 (Print) 1521-7388 (Online) Journal homepage: http://www.tandfonline.com/loi/uast20

Computational simulation of the dynamics of secondary organic aerosol formation in an environmental chamber

A. M. Sunol, S. M. Charan & J. H. Seinfeld

To cite this article: A. M. Sunol, S. M. Charan & J. H. Seinfeld (2018) Computational simulation of the dynamics of secondary organic aerosol formation in an environmental chamber, Aerosol Science and Technology, 52:4, 470-482, DOI: 10.1080/02786826.2018.1427209

To link to this article: https://doi.org/10.1080/02786826.2018.1427209

Accepted author version posted online: 16 Jan 2018.
Published online: 29 Jan 2018.

AEROSOL SCIENCE AND TECHNOLOGY
2018, VOL. 52, NO. 4, 470–482
https://doi.org/10.1080/02786826.2018.1427209

Computational simulation of the dynamics of secondary organic aerosol formation in an environmental chamber

A. M. Sunol, S. M. Charan, and J. H. Seinfeld

Division of Chemistry and Chemical Engineering, California Institute of Technology, Pasadena, California, USA

ABSTRACT

A key atmospheric process that is studied in laboratory chambers is the oxidation of volatile organic compounds to form low volatility products that condense on existing atmospheric particles (or nucleate) to form organic aerosol, so-called secondary organic aerosol. The laboratory chamber operates as a chemical reactor, in which a number of chemical and physical processes take place: gas-phase chemistry, transport of vapor oxidation products to suspended particles followed by uptake into the particles, deposition of vapors on the walls of the chamber, deposition of particles on the walls of the chamber, and coagulation of suspended particles. Understanding the complex interplay among these simultaneous physicochemical processes is necessary in order to interpret the results of chamber experiments. Here we develop and utilize a comprehensive computational model for dynamics of vapors and particles in a laboratory chamber and analyze chamber behavior over a range of physicochemical conditions.

ARTICLE HISTORY
Received 13 July 2017
Accepted 28 December 2017

EDITOR
Ilona Riipinen

1. Introduction

Understanding the chemical mechanisms by which volatile organic compounds (VOCs) are oxidized to low volatility products and secondary organic aerosol (SOA) is a major area of atmospheric chemistry research. The principal source of data on mechanisms of SOA formation is derived from laboratory chamber experiments, in which VOCs are caused to undergo oxidation, most frequently by the hydroxyl (OH) radical, to generate the low volatility products that condense into the particle phase (Schwantes et al. 2017). The SOA yield (Y) is determined as the ratio of the mass of organic aerosol formed to the mass of VOC reacted. To promote condensation of VOC oxidation products into the aerosol phase in the chamber, inert seed particles are customarily introduced to serve as sites for vapor condensation. Inevitably, the laboratory chamber contains walls, and interactions of vapors and particles with chamber walls must be accounted for in interpretation of data. For example, VOC oxidation products can condense onto growing aerosol or deposit onto the chamber wall, and even in the presence of seed aerosol, low volatility oxidation products may accumulate to a level at which they nucleate to form aerosol if the rate of generation of such products is sufficiently rapid to overcome the condensation sink. If an appreciable fraction of the VOC oxidation products deposits on the wall, then the SOA yield derived from the chamber data will be understated, perhaps significantly so. When such data are translated to the atmosphere, SOA yields would be correspondingly understated.

A common material used for flexible-walled environmental chambers is fluorinated ethylene propylene (FEP) Teflon film, customarily of thickness 0.05 mm. Irradiation of the chamber with actual or artificial sunlight is usually required to initiate photochemistry, and Teflon film has the attribute that it is essentially transparent to ultraviolet and visible radiation. From measurement of the size distribution of the aerosol suspended in the chamber over the course of an experiment, one can infer the mass of organic material that has condensed upon the original seed particles. There is ample evidence, however, that particles (Crump and Seinfeld 1981; McMurry and Grosjean 1985; McMurry and Rader 1985; Nah et al. 2017) and organic vapors (Matsunaga and Ziemann 2010; Yeh and Ziemann 2015; Zhang et al. 2015; Krechmer et al. 2016) can deposit on and adhere to Teflon chamber walls. To determine the SOA yield that would be produced in a "wall-less" chamber requires careful accounting for organic-containing

CONTACT J. H. Seinfeld seinfeld@caltech.edu Division of Chemistry and Chemical Engineering, California Institute of Technology, 1200 E California Blvd. 210-41, Pasadena, CA 91125, USA.

Color versions of one or more of the figures in the article can be found online at www.tandfonline.com/uast.

particles and low-volatility vapors that deposit on the chamber walls during the course of an experiment.

With recognition of the importance of competition between the suspended particles and the chamber wall for condensable vapors, strategies have been formulated to conduct VOC oxidation experiments using progressively higher concentrations of seed aerosol in order to enhance condensation of the low volatility vapors onto aerosol (Zhang et al. 2014; Nah et al. 2016, 2017). A consequence of this strategy is that, as the seed aerosol number concentration is increased, coagulation becomes increasingly important as a process affecting the aerosol size distribution (Pierce et al. 2008). The resulting complex coupling among aerosol condensational growth, wall deposition, and coagulation must be quantified.

The goal of the present work is to study numerically the temporal evolution of the vapor concentrations and the size- and composition-distributed aerosol in an environmental chamber undergoing gas-phase VOC oxidation over the range of parameter values characteristic of SOA formation. This includes particle growth by vapor condensation, deposition of vapor and particles to the chamber walls, and evolution of the particle size distribution due to simultaneous condensational growth and particle–particle coagulation. Several models exist based on numerical solution of the aerosol dynamic equations that address these phenomena. Meng et al. (1998) formulated a three-dimensional size-resolved and chemically resolved aerosol model, based in part on the work of Pilinis (1990), with gas-to-particle conversion represented by dynamic mass transfer between gas and aerosol phases. The model, which also includes explicit calculation of inorganic particle-phase thermodynamics, was applied to simulate gas and particle behavior in a 1987 air pollution episode in the South Coast Air Basin of California. Pierce et al. (2008) developed a model to simulate aerosol dynamics in a chamber involving simultaneous condensation, evaporation, coagulation, and wall deposition. The Pierce model was employed by Nah et al. (2016, 2017) to study effects of coagulation on particle wall deposition. Bian et al. (2015, 2017) used the TwO-Moment Aerosol Sectional (TOMAS) microphysics model (Adams and Seinfeld 2002; Pierce and Adams 2009; Pierce et al. 2011) to simulate organic species phase partitioning and particle and gas-phase wall losses during smog chamber characterization experiments involving wood smoke. The TOMAS model computes a size-resolved simulation of aerosol microphysics, conserving number and mass concentrations (see also Russell et al. 1998). Tian et al. (2017) derived a stochastic particle-resolved aerosol model (PartMC) that was applied to simulate coagulating ammonium sulfate particles in a cylindrical chamber, with special attention to fractal particle structure and wall loss. The computational model used in the present study is based on numerical solution of the aerosol dynamic equation (Seinfeld and Pandis 2016) to simulate particle growth by condensation, particle wall deposition, and coagulation, solved on a fixed particle size grid, with exact mass conservation of species.

2. Particle wall deposition

From the advent of environmental chambers, it was recognized that particles diffuse to and deposit on the chamber walls (Crump and Seinfeld 1981; McMurry and Grosjean 1985; McMurry and Rader 1985). Because the rate of particle deposition on the wall depends on the specific design parameters of each chamber (size, extent of mixing), the rate of wall deposition of particles as a function of particle size is generally determined experimentally by introducing particles of known sizes into the chamber, and after allowing time for mixing, measuring the size-dependent rates of wall deposition. The rate of deposition on the chamber walls is generally assumed to depend only on the particle size, so the rate of decay of the suspended particle number concentration distribution, $n_s(D_p, t)$, at diameter D_p is expressed as

$$\left(\frac{\partial n_s(D_p,t)}{\partial t}\right)_{\text{wallloss}} = -\beta(D_p)\; n_s\left(D_p,\, t\right) \qquad [1]$$

where the particle wall deposition coefficient $\beta(D_p)$ is determined by fitting the experimentally observed rates of decay of particles as a function of diameter.

If wall deposition is the sole process affecting aerosol number concentration in the chamber, determination of $\beta(D_p)$ from the rates of decay of particles of different sizes is relatively straightforward. However, if coagulation is appreciable, determination of $\beta(D_p)$ as solely representing particle wall deposition must account for the contribution of coagulation to the observed rate of particle decay. The dynamics of a suspended particle population $n_s(D_p,t)$ undergoing simultaneous coagulation and wall deposition is governed by

$$\begin{aligned}\frac{\partial n_s\left(D_p,t\right)}{\partial t} = {} & \frac{1}{2}\int_0^{D_p} K\left(\left(D_p^3-q^3\right)^{1/3}, q\right) \\ & n_s\left(\left(D_p^3-q^3\right)^{1/3}, t\right) n_s(q,t)\,dq \\ & - n_s\left(D_p,t\right)\int_0^{\infty} K\left(q,D_p\right) n_s(q,t)\,dq \\ & - \beta\left(D_p\right) n_s\left(D_p,t\right)\end{aligned} \qquad [2]$$

subject to the initial condition $n_s\left(D_p,0\right) = n_0\left(D_p\right)$, where $n_0\left(D_p\right)$ is the aerosol size distribution upon initial injection into the chamber, and $K\left(D_{p1}, D_{p2}\right)$ is the coagulation coefficient between particles of diameters

D_{p1} and D_{p2}. Determining the value of $\beta(D_p)$ in the presence of coagulation requires finding $\beta(D_p)$ such that the solution of Equation (2) subject to $n_0(D_p)$ matches as closely as possible to the observed aerosol dynamics in the chamber, $n_s(D_p, t)$.

The combination of gravitational settling and Brownian diffusion gives rise to a functional form of $\beta(D_p)$ that, at the small end of the particle size spectrum, decreases as D_p increases, owing to decreasing Brownian diffusion, and at the large particle end of the size spectrum, increases as D_p increases, owing to increased particle settling velocity. Whereas the result is a characteristic U-shaped function, the precise $\beta(D_p)$ functionality must be determined experimentally for each chamber. An advantageous approach to determining $\beta(D_p)$ is to specify a $\beta(D_p)$ function having the proper characteristic functionality, with a set of unknown parameters to be determined by optimal fitting of the numerical solution of Equation (2) to the observed size distribution dynamics in the chamber in question (Pierce et al. 2008; Nah et al. 2017). This procedure requires iterative numerical solution of Equation (2), such that each revised set of parameters characterizing $\beta(D_p)$ moves the calculated $n_s(D_p, t)$ closer to the experimentally observed $n_s(D_p, t)$, as measured by a performance criterion of closeness of calculated $n_s(D_p, t)$ to observed $n_s(D_p, t)$.

The goal is to minimize the objective function,

$$J[\beta(D_p)] = \int_0^{t_f} \int_{D_{p,l}}^{D_{p,u}} [n_{s,\,obs}(D_p, t) - n_{s,\,pred}(D_p, t)]^2 dD_p dt \quad [3]$$

where $n_{s,\,obs}(D_p, t)$ is the observed size distribution and $n_{s,\,pred}(D_p, t)$ is that predicted using an assumed functional form of $\beta(D_p)$, here assumed to be

$$log_{10}[\beta(D_p)] = a + b log_{10}(D_p) + c[log_{10}(D_p)]^2 + d[log_{10}(D_p)]^3 \quad [4]$$

where a, b, c, d are the parameters that characterize $\beta(D_p)$. Before an optimal $\beta(D_p)$ is found from the minimization of $J[\beta(D_p)]$ in Equation (3), an initial guess for the four parameters (a, b, c, and d) must be chosen.

To evaluate the performance of the minimization of J, we performed 20-h simulations of simultaneous coagulation and wall deposition of an aerosol introduced into a chamber at $t = 0$ (Figure 1). $n(D_p, t)$ was discretized into 50 logarithmically distributed bins with mean diameters between 50 and 1,000 nm. The method for finding the initial guess is shown visually and explained in Figure 2 and its caption. Randomly distributed measurement uncertainty of 5% was added to particle number concentrations in each bin. Figure 3 shows the results of optimization for 20 different simulations, each of these with the same base data but different realizations of the 5% measurement uncertainty.

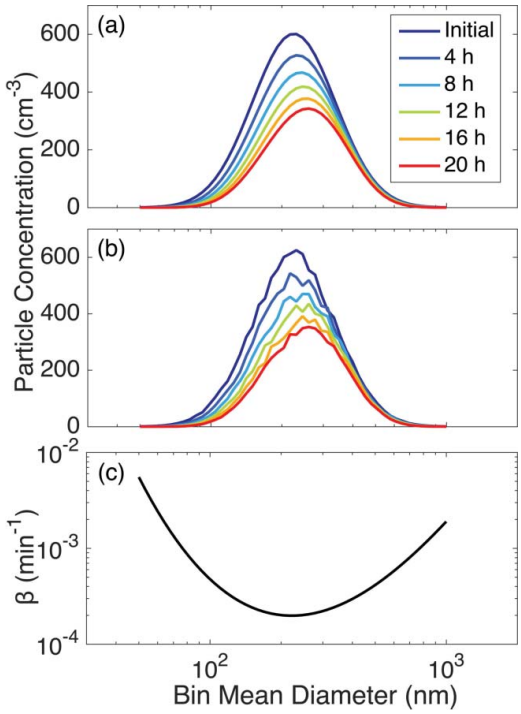

Figure 1. (a) and (b) show the evolution of a particle size distribution undergoing coagulation and particle wall deposition over 20 h for an initially lognormal distribution, assuming $\beta(D_p)$ shown in (c). The initial total number concentration is 10^4 cm^{-3}, and the initial lognormal distribution is centered at 225 nm with σ_g = 1.5. The mean diameters of the 50 bins are lognormally distributed between 50 and 1,000 nm. Data in (b) were generated by applying ±5% measurement uncertainty to the number concentration in each of the 50 bins.

3. Chamber physics and chemistry

3.1. Particle growth

During SOA formation, each particle that deposits on the wall of an environmental chamber carries with it the condensed organic mass from the inception of the experiment. In order to account for that particle-borne organic material in computing the overall SOA yield, it is necessary to keep track of particle size (and therefore the amount of condensed organic) upon deposition. Since the extent to which deposited particles continue to interact with the gas-phase contents of the chamber is unknown, two limiting assumptions have been invoked to estimate the contribution of the deposited particles to the amount of SOA (Hildebrandt et al. 2009; Loza et al. 2010): (1) The "lower bound" assumption states that once particles deposit on the wall, they cease interacting with the vapor

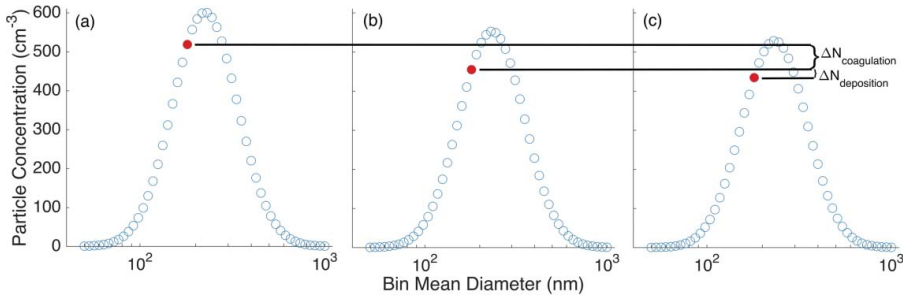

Figure 2. Process for choosing an initial guess for $\beta(D_p)$. The solid (red) dots represent the number concentration in the same size bin in all three distributions. (a) and (c) represent data points at times t_1 and t_2, respectively. When used to find an initial guess, time increments ($t_2 - t_1$) were chosen to be 6.5 min; in this figure, the time increment is 4 h, so that the procedure is visually obvious. (b) A simulation for one time increment with the distribution at t_1 as the initial condition and with $\beta(D_p) = 0$. Since (b) corresponds to a system in which particles from the distribution at t_1 are allowed to coagulate but not to deposit on the wall, the difference between the number concentration of a specific size bin from the t_2 distribution, shown in (b), and from the actual distribution at t_2, shown in (c), is then denoted $\Delta N_{\text{Deposition}}$. $\beta(D_p)$ is next calculated as $\beta(D_p, t_{1/2}) = \frac{\Delta N_{Deposition}}{N_{t_1}(t_2 - t_1)}$. A mean $\beta(D_p)$ can be found by averaging these values for a specific D_p over all the time points where the initial distribution has arbitrarily >10 particles cm^{-3} for that size bin. These average $\beta(D_p)$ values are next fit to the function in Equation (4) and these values of *a*, *b*, *c*, and *d* are used as an initial guess for the determination of $\beta(D_p)$.

in the chamber; and (2) The "upper bound" assumes that wall-deposited particles continue to absorb vapor as if they had remained suspended. Thus, the upper bound assumption is identical to that if the particles were still suspended. In treating the continued uptake of vapor by particles that have deposited on the chamber wall, one must assume an appropriate particle surface area for mass transport. The assumption made here is that, after deposition on the wall, the particle retains its spherical shape, and therefore its surface area remains the same as if it were still suspended. For a discussion of assumptions concerning the nature of deposited particles, the reader is referred to Trump et al. (2016).

The rate of vapor uptake by a particle is described in terms of the mass accommodation coefficient α_p, which is defined as the fraction of incoming vapor molecules that is taken up by the particle (Julin et al. 2014; Zhang et al. 2015). The mass accommodation coefficient α_p can be defined as either surface (α_{ps}) or bulk (α_{pb}) accommodation coefficient (Kolb et al. 2010), the difference being the extent to which the condensing molecule needs to be incorporated in the particle bulk to be considered as accommodated. Molecular-level simulations of molecule–surface interactions can distinguish between surface and bulk accommodation (Julin et al. 2014), but typical vapor–particle interactions in a laboratory chamber tend to be represented by a single overall mass accommodation coefficient, α_p. Rapid equilibration of an incoming vapor between the gas and particle phases is a reasonable assumption for a liquid-phase particle (Shiraiwa and Seinfeld 2012), although if the particle is solid or semisolid or if particle-phase chemistry plays an influential role in uptake, accommodation can be retarded. From a macroscopic point of view, the value of α_p for a particular vapor–aerosol system is determined by fitting observed aerosol growth rate data to a dynamic growth model.

Particle-phase accretion reactions can produce effectively nonvolatile products. Such products can lead to an increase in the viscosity of the particle and reduced particle-phase diffusivity, retarding evaporation, and inhibiting gas–particle partitioning (Virtanen et al 2010a, b; Vaden et al. 2010, 2011; Abramson et al. 2013; Zaveri et al. 2014). In such a case, the timescale to achieve gas–particle equilibrium, $\tau_{g,p}$, may be long compared to the timescales for achieving gas–wall partitioning and for VOC oxidation, $\tau_{g,w}$ and τ_{rxn} (Zhang et al. 2012; Shiraiwa and Seinfeld 2012; Shiraiwa et al. 2013; Mai et al. 2015). Retarded gas–particle partitioning resulting from slow condensed-phase diffusion of vapor molecules will drive the vapor–particle system toward so-called *kinetically limited growth*. A vapor–particle accommodation coefficient, α_p, of order, say, 10^{-3}, leads to a vapor–particle equilibration timescale that is competitive with or can exceed that associated with the rate of change of vapor concentration due to both vapor-phase oxidation and vapor wall loss. When the production rate of condensable vapors is slow compared to the time needed to establish gas–particle equilibrium, the system exhibits *quasi-equilibrium growth.*

The magnitude of the timescale needed to establish gas–particle equilibrium, $\tau_{g,p}$, relative to the timescales for other processes in the system governs the extent to which the system is characterized by kinetically limited versus quasi-equilibrium growth. Gas–particle equilibrium is governed by the total organic mass in the system and is not explicitly dependent on the aerosol surface area. In contrast, kinetically limited condensation, for which $\tau_{g,p}$ is competitive with the timescale for VOC oxidation, depends on the aerosol surface area. The

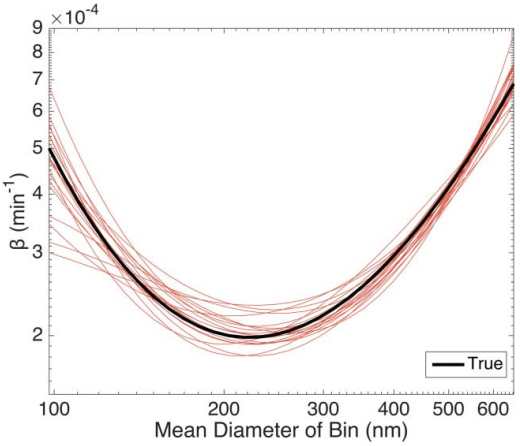

Figure 3. Optimization procedure to determine $\beta(D_p)$. The full optimization procedure to determine $\beta(D_p)$ was performed 20 times and each thin (red) curve represents one of these converged functions. Each of the optimized $\beta(D_p)$ functions was determined by taking the number concentrations in all of the 50 size bins shown in Figure 1a and subjecting these to a ±5% random; an example of the data used as an input is shown in Figure 1b. Once an initial guess of *a, b, c*, and *d* was found (the method for which is shown in Figure 2), these four parameters were used to minimize the function $J\left(\beta\left(D_p\right)\right)$ in Equation (3). An average of 290 iterations were required for the optimization to converge. These values of *a, b, c*, and *d* then give the determined $\beta(D_p)$, which is shown as a thin (red) curve. In actual chamber experiments, the true value of $\beta(D_p)$ is unknown; using the method described here produces the set of thin (red) curves. To assess the performance of this method, we applied this procedure with simulated data with an assumed, true value of $\beta(D_p)$, which is shown both in Figure 1c and here in bold (black) to visually aid the comparison to each of the thin (red) lines. The range for the *x*-axis includes only bins with a number concentration $>10\ \mathrm{cm}^{-3}$ for the duration of the 20-h experiment.

timescale for the production of condensable vapors, τ_{rxn}, is generally estimated on the basis of k_{rxn} [OH]. If $\tau_{g,p} > \tau_{rxn}$, condensation is kinetically limited. As α_p increases toward unity, $\tau_{g,p}$ decreases with respect to τ_{rxn}, and condensation shifts toward quasi-equilibrium growth.

3.2. Idealized kinetics

The essential characteristics of the gas-phase oxidation of a VOC to form SOA are the timescale of oxidation and the progression to lower volatility oxidation products. As a means of representing gas-phase kinetics in the simulations to follow, we use the idealized first-order kinetic scheme of McVay et al. (2014):

$$\mathrm{A} \xrightarrow{k_1} \mathrm{B} \xrightarrow{k_2} \mathrm{C} \xrightarrow{k_3} \mathrm{D}$$

In this scheme, A represents the completely volatile parent VOC, and B, C, and D represent oxidation products, with successively decreasing volatility. The magnitudes of the effective first-order rate constants, k_1, k_2, and k_3, govern the overall chemical reaction timescale of the system. The volatilities of the oxidation products are represented by their saturation mass concentrations, C_B^*, C_C^*, and C_D^*. In the present study, we do not consider particle-phase chemistry involving condensed B, C, and D. One could hypothesize generalized particle-phase reactions involving condensed B, C, and D that would further decrease (or possibly increase) the volatility of the aerosol, but this aspect is left for future work, especially in the case in which explicit particle-phase chemistry is established.

3.3. Vapor wall deposition

Vapor molecules in the generally well-mixed core of a chamber are transported through a boundary layer adjacent to the walls by a combination of molecular and turbulent diffusion (Zhang et al. 2015; Ye et al. 2016; Trump et al. 2016). As a vapor molecule *i* reaches the chamber wall, the fraction of encounters that lead to uptake is represented by the vapor wall accommodation coefficient, $\alpha_{w,i}$, which depends on the nature of the wall surface as well as the chemical composition of the species. Vapor species that deposit on the wall, in principle, may re-evaporate, eventually leading to an equilibrium between the gas phase and the wall. The absorptive nature of the wall has been characterized by a parameter defined as the equivalent absorbing organic mass on the wall, C_w (Matsunaga and Ziemann 2010; Yeh and Ziemann 2015). For an FEP Teflon-walled chamber, the quantity C_w can be regarded as characterizing the equilibrium solubility of individual vapor molecules in FEP Teflon polymer.

The rate of uptake of vapors by the wall can be characterized by the overall first-order vapor wall deposition coefficient, k_w, which depends on the surface area-to-volume ratio of the chamber, the degree of mixing in the chamber, the rate of gas-phase diffusion across the wall layer, and the vapor-wall accommodation coefficient, $\alpha_{w,i}$ (Zhang et al. 2015). The timescale characterizing the vapor wall deposition process is $\tau_{g,w} = {k_w}^{-1}$.

The rate of deposition of vapor to the chamber walls is represented as a first-order process, characterized by the first-order rate coefficient, k_w (s^{-1}) (Zhang et al. 2015). Vapor wall deposition is assumed to be reversible, with the vapor-wall partitioning coefficient, K_w:

$$K_w = \frac{R\ T}{M_w\ \gamma_w\ P_{sat}} \qquad [5]$$

Here R is the ideal gas constant, T is temperature, M_w is the effective molecular weight of the absorbing wall material, γ_w is the effective activity coefficient of

the dissolved material in the wall, and P_{sat} is the saturation vapor pressure of the species of interest. Oxidation products, B, C, and D, are considered to condense on suspended particles as well as deposit reversibly onto the chamber walls. The governing equation for the concentration of a suspended vapor, such as B, is:

$$\frac{dB_g}{dt} = -k_{w,on,B}B_g + k_{w,off,B}B_w + k_1A_g - k_2B_g - J_B \quad [6]$$

where, $k_{w,on}$ and $k_{w,off}$ (s^{-1}) are the first-order rate coefficients for deposition on and evaporation from the wall, k_1 and k_2 are the oxidation rate constants of A and B, B_g and B_w are the concentrations of B suspended and on the wall, respectively, and J_B is the condensation rate of B onto particles. Vapor molecules are transported both to and from the wall. We express K_w in terms of $k_{w,on}$ and the first-order evaporation coefficient $k_{w,off}$. $k_{w,on}$ and $k_{w,off}$ are related through

$$K_wC_w = \frac{k_{w,on}}{k_{w,off}} \quad [7]$$

$k_{w,on}$ represents the overall rate of transport of vapor species from the core of the chamber to the edge of the wall boundary layer and through the boundary layer by molecular diffusion (McVay et al. 2014; Zhang et al. 2015),

$$k_{w,on} = \left(\frac{A}{V}\right)\frac{\frac{\alpha_w\,\bar{c}}{4}}{1+\frac{\pi}{2}\left(\frac{\alpha_w\,\bar{c}}{4\sqrt{k_e\,D_i}}\right)} \quad [8]$$

$$k_{w,off} = \frac{k_{w,on}\;C^*}{C_w} \quad [9]$$

Here A/V is the surface area to volume ratio of the chamber; α_w is the mass accommodation coefficient of vapor species on the wall; k_e is the eddy diffusion coefficient for mixing in the chamber; D_i is the molecular diffusivity of the vapor in the thin layer adjacent to the wall; $\bar{c}$ is the mean thermal speed of the vapor, assumed for convenience to be the same for B, C, and D; C_w is the effective wall organic aerosol concentration; and C_i^* is the saturation mass concentration for species i. As noted earlier, C_w is the parameter that represents the capacity of the Teflon material itself to absorb organic molecules. Typical values of D_i and $\bar{c}$ for the classes of molecules important in SOA formation are $\sim 3 \times 10^6$ m^2 s^{-1} and 200 m s^{-1}, respectively. Values of k_e ranging from 10^{-3} to 1 s^{-1} correspond to chamber mixing timescales of 17 min to 1 s. A mixing timescale of 10^{-3} s^{-1} is characteristic of that in a typical chamber of volume exceeding $\sim$20 m^3.

3.4. Aerosol conservation equation

The overall governing conservation equation for the suspended aerosol size distribution $n_s(D_p, t)$ is as shown below:

$$\frac{\partial n_s(D_p,t)}{\partial t} = \left(\frac{\partial n_s(D_p,t)}{\partial t}\right)_{\text{coagulation}} + \left(\frac{\partial n_s(D_p,t)}{\partial t}\right)_{\text{condensation}} + \left(\frac{\partial n_s(D_p,t)}{\partial t}\right)_{\text{wallloss}} \quad [10]$$

The rate of condensation of vapor molecules onto particles is given by:

$$J_i = 2\pi D_iD_p\left(G_i - G_i^{eq}\right)F_{FS} \quad [11]$$

where G_i is the gas-phase concentration of species i, G_i^{eq} is the equilibrium gas-phase concentration over a particle, and F_{FS} is the Fuchs–Sutugin correction factor for noncontinuum gas-phase diffusion (Seinfeld and Pandis 2016),

$$F_{FS} = \frac{0.75\;\alpha_p\;(1+Kn)}{Kn^2+Kn+0.283\;Kn\;\alpha_p+0.75\;\alpha_p} \quad [12]$$

The rate of change of the suspended aerosol size distribution owing to vapor condensation on suspended particles is:

$$\left(\frac{\partial n_s(D_p,t)}{\partial t}\right)_{\text{condensation}} = -\frac{\partial}{\partial D_p}\left[I\left(D_p,\,t\right)n_s\left(D_p,\,t\right)\right] \quad [13]$$

where $I(D_p, t)$ is the rate of change in particle diameter due to condensation or evaporation.

3.5. Key parameters

The principal parameter that controls the rate of particle growth by vapor condensation is α_p, the accommodation coefficient of a vapor species on particles. As noted earlier, α_p has been found to vary over the range of $\sim$0.001 to close to 1.0 for different VOC systems (McVay et al. 2014). A related parameter, α_{pw}, describes the growth by vapor condensation of particles that have deposited on the wall. Of the two limiting assumptions that describe the growth of particles that have deposited on the wall, we adopt the lower bound assumption, in which once particles are lost to the walls, vapor condensation to these particles ceases, in which case, $\alpha_{pw} = 0$.

The oxidation rates of the vapor species, A, B, and C, as embodied in the first-order rate coefficients k_1, k_2, and k_3, establish the overall time scale for the temporal behavior of the system. The nominal initial oxidation rate constant for the simulations to be presented subsequently is $k_1 = 10^{-4}$ s^{-1}, with each subsequent oxidation rate coefficient assumed to increase by a factor of five. Vapor wall deposition is represented by the principal parameters, C_w the effective wall organic aerosol concentration, and α_w, the accommodation coefficient of vapor species onto the wall. The nominal value of α_w is assumed to be 10^{-5}. Matsunaga and Ziemann (2010) estimated a range of values, C_w = 2, 4, 10, and 24 mg m^{-3} for alkanes, alkenes, alcohols, and ketones. The nominal value used in the numerical studies here is C_w = 10 mg m^{-3}. Nominal values of parameters are summarized in Table 1, together with ranges used in simulations.

The size distribution of the seed aerosol at the start of an experiment is assumed to follow a log-normal distribution centered at a diameter of 225 nm, with geometric standard deviation $\sigma_g = 1.5$. The initial number concentration of seed particles is a key experimental variable. The base value of the initial seed number concentration is taken as 10^4 cm^{-3}.

3.6. Computational model

The computational model tracks the evolution of the particle size distribution in the chamber over time, and that of the gas-phase concentrations of A, B, C, and D, as well as the fraction of each that is suspended or on particles/the wall. Because the stoichiometric coefficients in the idealized gas-phase chemistry have been chosen to be unity, given adequate time in the chamber and the absence of wall deposition of particles or vapor, the theoretical maximum yield of SOA (the mass of SOA formed per mass of A reacted) that can be achieved is 1.0. Simulations are carried out for an experimental time of 20 h.

4. Computational simulations

The focus of the present work is exploring the relative importance of the physicochemical processes involving vapor molecules and particles in an environmental chamber, with particular attention to those competitive processes that arise as a consequence of the chamber itself. Here we present a range of simulations in which physicochemical parameters are systematically varied. Whereas there are several metrics that could be used to assess the characteristics of a particular chamber experiment, the SOA yield, Y, attained over a fixed experimental duration serves as the overall measure of the performance of the system.

4.1. Simultaneous vapor condensation on particles and vapor and particle deposition on chamber walls

Figure 4 shows the effect of variation of key parameters on SOA yield. Y increases as α_p increases since vapor condenses onto particles more readily (Figure 4a), and Y becomes less sensitive to α_p as α_p approaches unity. At the limit $\alpha_p = 1$, Y is only mildly sensitive to the value of α_w (Figure 4b) since vapor condensation on particles proceeds at its maximum rate; at $\alpha_p = 0.001$ a considerable portion of the vapor remains suspended for a longer period of time, and is therefore subject to vapor wall deposition, leading to a strong effect of increasing α_w on Y. As C_w decreases (Figure 4c), the capacity of the wall to take up vapor decreases, increasing Y. As the rate constants for A → B → C → D increase (Figure 4d), over a fixed experimental time, Y increases rapidly as α_p increases owing to the greater availability of lower volatility oxidation products, B, C, and D. As the values of C_B^*, C_C^*, and C_D^* decrease (Figure 4e), the overall lower volatility of oxidation products leads to an increase in Y, although at $\alpha_p = 0.001$, that increase is modest, since the value of α_p exerts a stronger control on Y than does the volatility C^*, at the assumed values of C_B^*, C_C^*, and C_D^*. Y increases as the initial number concentration of particles (Figure 4f) increases, particularly for $\alpha_p = 0.001$. This is

Table 1. Chamber parameters.

Parameter	Definition	Base value	Range of values considered
α_p	Accommodation coefficient of vapor species on suspended particles	10^{-3}	10^{-3} to 1
α_{pw}	Accommodation coefficient of vapor species on particles deposited on the wall	0	0 and α_p
α_w	Accommodation coefficient of vapor species deposited on the wall	10^{-5}	10^{-7} to 10^{-4}
k_1	First-order oxidation rate constant for A	1×10^{-4} s^{-1}	1×10^{-6} to 1×10^{-3} s^{-1}
k_2	First-order oxidation rate constant for B	5×10^{-4} s^{-1}	5×10^{-6} to 5×10^{-3} s^{-1}
k_3	First-order oxidation rate constant for C	25×10^{-4} s^{-1}	25×10^{-6} to 25×10^{-3} s^{-1}
C_w	Effective wall organic aerosol concentration	10 mg m^{-3}	10^{-2} to 10 mg m^{-3}
C_B^*	Saturation mass concentration for species B	10 μg m^{-3}	10^{-1} to 10^2 μg m^{-3}
C_C^*	Saturation mass concentration for species C	1 μg m^{-3}	10^{-2} to 10 μg m^{-3}
C_D^*	Saturation mass concentration for species D	10^{-1} μg m^{-3}	10^{-3} to 1 μg m^{-3}
N_t	Initial total number concentration of seed particles	10^4 cm^{-3}	10^3 to 10^6 cm^{-3}

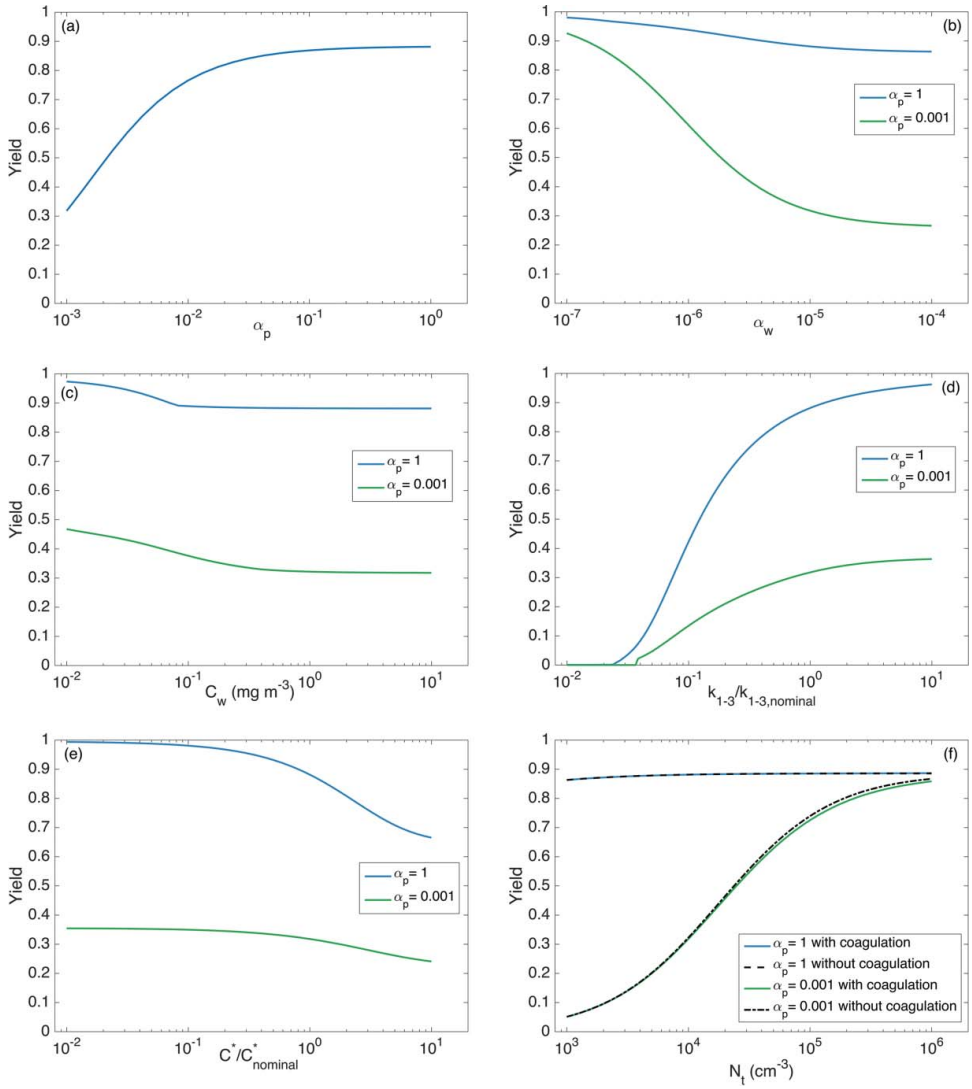

Figure 4. Secondary organic aerosol (SOA) yield Y for nominal parameter values in Table 1 with coagulation occurring. (a) α_p; (b) α_w; (c) C_w; (d) k_1; k_2; k_3; (e) C_B^*; C_C^*; C_D^*, (f) N_t. In (f), both the presence and absence of coagulation are considered.

because an increase in number concentration increases the suspended surface area and so preferences condensation onto suspended particles. When $\alpha_p = 1$, there is less competition in condensation between the wall and the suspended particles, so the effect of an increase in suspended surface area is dampened: since condensation onto suspended particles is already dominating condensation onto the walls, the change in this surface area due to coagulation – while still quite small – is noticeable, that is, in the absence of coagulation, the total available suspended surface area decreases since all particles are modeled as spheres.

The effect of α_p (0.001 vs. 0.01 vs. 1.0) on the distribution of products B, C, and D at the end of the experiment is shown in Figure 5. Under conditions of $\alpha_p = 0.001$, at the end of the simulation (Figure 5a), the majority of species B, C, and D is predicted to have deposited on the chamber wall. An increase in α_p by a factor of 10 to 0.01 (Figure 5b) has a substantial effect on the distribution of B, C, D, as Y is predicted to increase from 0.32 to 0.77. At $\alpha_p = 1$ (Figure 5c), the majority of products B, C, and D reside on suspended particles, and Y has increased to 0.88. In all three cases, little of the products reside in particles that have deposited on the chamber wall, owing to the fact that the surface area of deposited particles is much less than that of the suspended. There is little difference between the cases of $\alpha_p = 0.1$ and $\alpha_p = 1$ (not shown); an accommodation coefficient of 0.1 is essentially equal to $\alpha_p = 1.0$ in terms of the effect on the distribution of products.

Decreasing α_w (10^{-7} vs. 10^{-5}) at $\alpha_p = 0.001$, as seen in Figure 6, produces a dramatic change of product distribution Y from that at $\alpha_w = 10^{-5}$. At $\alpha_w = 10^{-7}$, the majority of B, C, and D are predicted to reside on suspended particles, and $Y = 0.93$ versus 0.32, with virtually no suspended vapor left in the chamber. For $\alpha_w > 10^{-5}$,

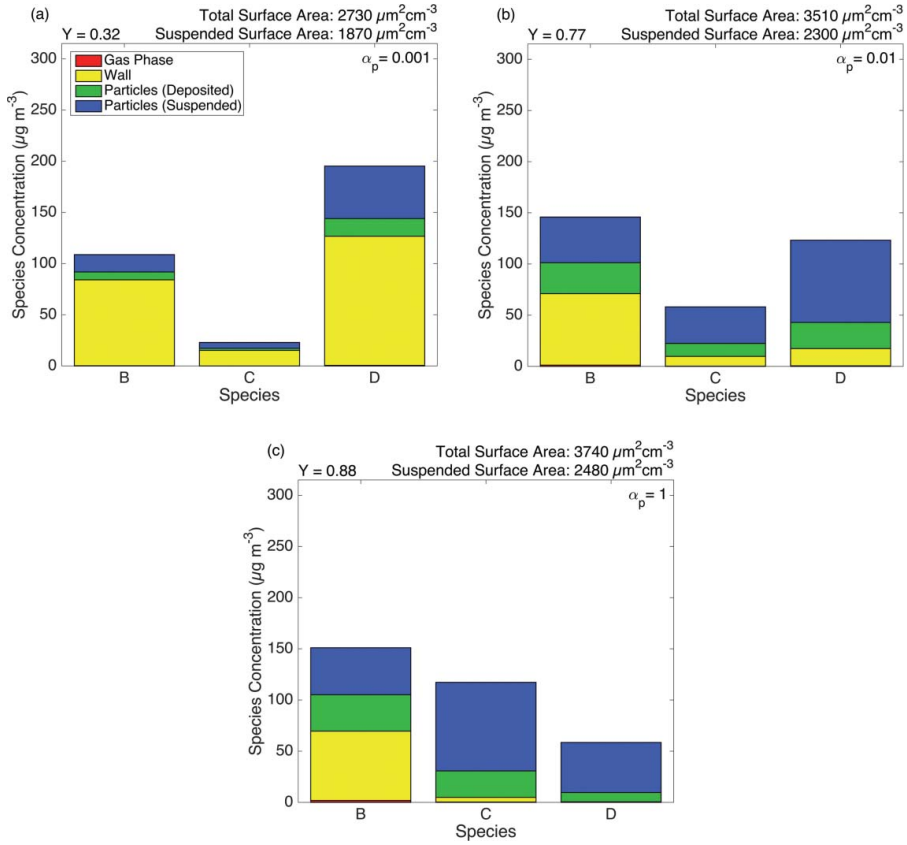

Figure 5. Variation of the distribution of oxidation products B, C, and D among suspended vapor, wall deposited vapor, suspended particles, and wall deposited particles for the nominal parameter values in Table 1. (a) $\alpha_p = 0.001$; (b) $\alpha_p = 0.01$; (c) $\alpha_p = 1.0$.

there is little change in the distribution of B, C, and D from that at $\alpha_w = 10^{-5}$ (not shown).

The effect of increased oxidation rate on the distribution of B, C, and D at the end of the simulated experiment for $\alpha_p = 0.001$ is shown in Figure 7. The nominal values of k_1, k_2, and k_3 are 0.0001 , 0.0005, and 0.0025 s^{-1}, respectively; at a factor of 10 increase, $k_1 = 0.001$ s^{-1}, $k_2 = 0.005$ s^{-1}, and $k_3 = 0.025$ s^{-1}, conversion of A to D occurs an order of magnitude more rapidly. This accelerated rate of conversion is not, however, accompanied by a concomitant increase in Y. Comparing Figures 5a and 7a, we note that Y increases only from 0.32 to 0.36. The explanation for this modest increase in Y can be attributed to the value of $\alpha_p = 0.001$; despite an order of magnitude increase in reaction rates, the low accommodation rate of vapor on particles ($\alpha_p = 0.001$) exerts the dominant influence on Y. When the order of magnitude increase in k_1, k_2, and k_3 occurs at $\alpha_p = 1.0$ (Figure 7b), the so-called *kinetic effect* is clearly demonstrated, with the overall Y increasing from 0.36 (Figure 7a) to 0.96 (Figure 7b).

Since α_{pw} is set to 0 throughout all the simulations described, the compounds are found on deposited particles only when they condense on suspended particles and these particles later deposit on the chamber walls. Since increasing the oxidation rate shifts the condensation of compounds onto particles earlier in the experiment – when there are still numerous particles present – more of the compounds end up on particles that later deposit on the walls.

Experimental evidence suggests that C_w is likely to be relatively large (Matsunaga and Ziemann 2010). At values near the nominal value of $C_w = 10^4$ μg m^{-3}, Y does not vary appreciably for modest changes in C_w, but does vary significantly for values lower than the nominal value (Figure 4c). Y is most sensitive to C_w when the value of C_w is in the vicinity of that of C_{OA} (the concentration of organics). The effect of the value of C_w on Y is addressed in Figure 8. If C_w is decreased from its nominal value of 10^4 to 10 μg m^{-3}, at $\alpha_p = 0.001$ and $\alpha_w = 10^{-5}$, Y increases to 0.47 (Figure 8) from 0.32 (Figure 5a). At $\alpha_p = 1$, Y increases from 0.88 at $C_w = 10^4$ μg m^{-3} to 0.97 at $C_w = 10$ μg m^{-3} (distributions of B, C, D not shown).

The predicted value of Y corresponding to the two limiting assumptions regarding the extent to which particles on the wall continue to take up vapor can be assessed. We considered the distribution of B, C, D, in the two limiting cases in which wall-deposited particles either continue to or do not absorb vapors. For $\alpha_p = 0.001$, Y with ($\alpha_{pw} = \alpha_p$) and without particles in the wall growing is, respectively, 0.33 and 0.32. At $\alpha_p = 1.0$, $Y = 0.91$ for $\alpha_{pw} = 1$ and 0.88 for

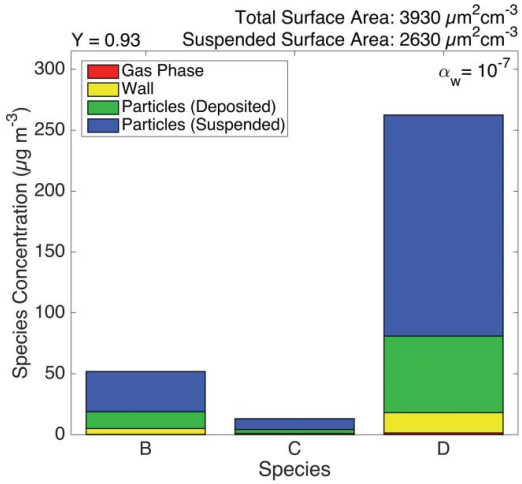

Figure 6. Variation of the distribution of oxidation products B, C, and D among suspended vapor, wall deposited vapor, suspended particles, and wall deposited particles for parameter values in Table 1 except for $\alpha_w = 10^{-7}$. By comparison with Figure 5a, note the strong effect of a two order of magnitude decrease in α_w on the distribution of B, C, and D among the suspended particles, wall deposited vapor, and deposited particles.

$\alpha_{pw} = 0$. These results demonstrate the relatively small difference in Y between the so-called upper and lower limit assumptions concerning the extent to which particles deposited on the wall continue to absorb vapors.

4.2. Effect of coagulation

Implementation of increasingly higher number concentrations of seed aerosol as a means to stimulate preferential condensation of vapor on particles is accompanied by increasing influence of coagulation on the dynamics of the particle size distribution (Nah et al. 2016, 2017). Also, as particles in the chamber grow due to accretion of vapor oxidation products, the overall rate of wall deposition of particles evolves, in accordance with the particle size dependence of the wall deposition function, $\beta(D_p)$. Coagulation occurs simultaneously with particle growth, also serving to shift the overall particle size distribution to larger diameters, at the same time accompanied by a reduction in the overall particle number concentration. Coagulation leads to a decrease in the overall surface area of the suspended particles, since there are fewer particles, and because particles grow into sizes for which the deposition rate $\beta(D_p)$ is larger. The overall decrease in surface area is, therefore, a combined result of coagulation and increased wall deposition.

Vapor deposition on the walls of the chamber is controlled by the two parameters, α_w and C_w. Particles that deposit onto the wall serve to decrease both the amount of suspended oxidized products and the overall rate of condensation. Moreover, as N_t is increased with all other conditions the same, Y increases, since the effect of vapor wall loss is diminished, and at higher α_p, condensation competes more favorably with vapor wall deposition, leading to higher Y. In simulations carried out in the presence and absence of coagulation (not shown), coagulation has a modest effect on Y at high seed concentrations and low α_p. Furthermore, comparison of simulations with small and large mean diameters (D_{pg} = 100 and 400 nm) shows that coagulation has a larger effect on smaller diameter particles (not shown).

4.3. Kinetically limited versus quasi-equilibrium growth

The extent to which SOA yield increases with increasing seed aerosol surface area depends on the nature of the VOC oxidation system. In the toluene photoxidation system, Zhang et al. (2014) showed that Y

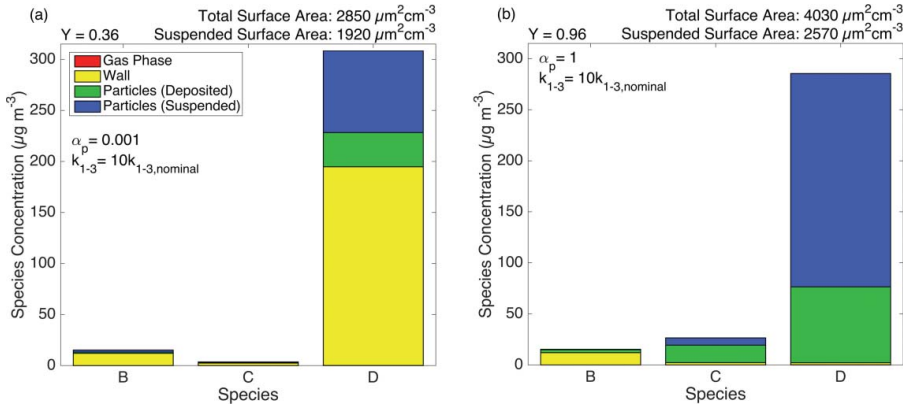

Figure 7. Variation of the distribution of oxidation products B, C, and D among suspended vapor, wall deposited vapor, suspended particles, and wall deposited particles for a tenfold increase in k_1, k_2, and k_3 over the nominal values at $\alpha_p = 0.001$ (a) and $\alpha_p = 1.0$ (b). For (a), the retarded rate of condensation of B, C, and D on suspended particles leads to an accumulation of wall deposited vapor and Y = 0.36, whereas for (b), the lack of retardation of condensation leads to $Y = 0.96$.

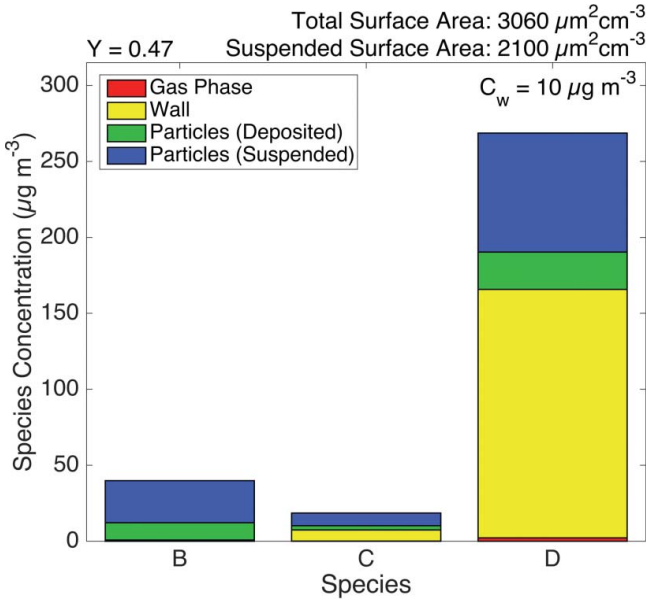

Figure 8. Variation of the distribution of oxidation products B, C, and D among suspended vapor, wall deposited vapor, and particles for $\alpha_p = 0.001$ and $C_w = 10$ μg m^{-3}. At $\alpha_p = 0.001$, the difference in Y corresponding to $C_w = 10$ μg m^{-3} and $C_w = 10^4$ μg m^{-3} (see Figure 5a) is a decrease from 0.47 to 0.32, reflecting the capacity of the wall to take up vapors.

increases with increasing seed aerosol surface area, whereas Nah et al. (2016) found in the α-pinene ozonolysis system that SOA growth rate and Y are essentially independent of seed surface over the range of seed surface area studied. Moreover, McVay et al. (2014) showed that Y depends on seed aerosol surface area only in systems in which the condensation of SOA-forming vapors onto seed aerosol particles is kinetically limited, that is, the timescale to establish gas–particle equilibrium is competitive with or greater than the timescales for VOC oxidation and vapor wall deposition. In addition to seed aerosol surface area, VOC oxidation rate may also play an important role in establishing the effect of vapor wall deposition on SOA formation, with more rapid oxidation leading to higher Y. This is a consequence of the competition between growing particles and chamber walls for condensable VOC oxidation products. In the α-pinene ozonolysis SOA system of Nah et al. (2016), the best fit α_p value of 0.1 (or 1 with essentially the same statistical error) is consistent with the absence of significant limitations to vapor particle mass transfer, for which SOA formation is governed by quasi-equilibrium growth (Saleh et al. 2013; McVay et al. 2014).

The key parameter controlling the competition between the seed aerosol surface area effect and the oxidation rate effect is α_p (Figure 9). In general, for $\alpha_p \sim 0.1$ to 1.0 (Figure 9a has $\alpha_p = 1.0$), the oxidation rate dominates, and Y increases significantly as the VOC oxidation rate increases, while seed aerosol surface area has a negligible effect. For $\alpha_p = 0.001$ (Figure 9b), both effects can be observed: at low oxidation rate and high seed aerosol surface area, the oxidation rate effect dominates; at low seed aerosol surface area and rapid oxidation rate, the seed surface area dominates. In summary, the magnitude by which vapor wall deposition affects SOA yield depends on the extent to which the VOC system is characterized by kinetically limited SOA condensation growth. For either large α_p or large N_t, the chamber is effectively saturated with particles in terms of its competitiveness with the oxidation rate, so neither changing has much of an effect on Y. When comparing the cases in the presence and absence of coagulation (not shown), overall SOA yields are predicted to be lower in the presence of coagulation, owing to the decrease of the overall surface area of particles available for vapor condensation.

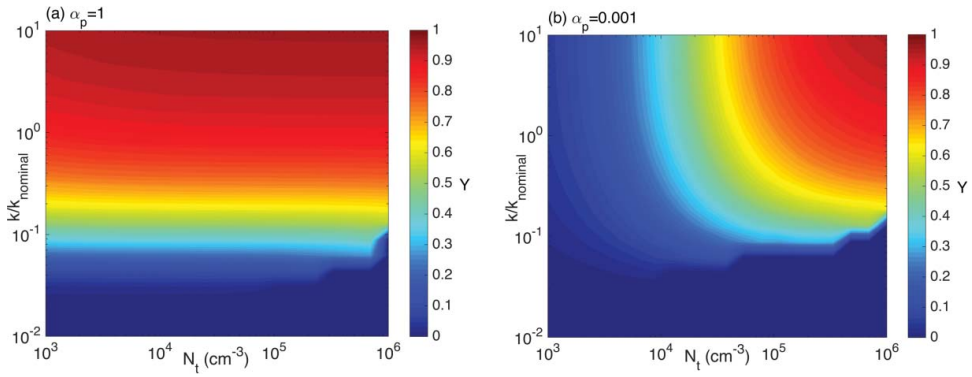

Figure 9. SOA yield as a function of initial seed concentration, N_t, and the oxidation rate, k, where the nominal oxidation rates are $k_1 = 0.0001$ s^{-1}, $k_2 = 0.0005$ s^{-1}, and $k_3 = 0.0025$ s^{-1}. For (a) $\alpha_p = 1.0$, the oxidation rate dominates since N_t has a negligible effect on Y. For (b) $\alpha_p = 0.001$, the oxidation rate dominates at low oxidation rates but the seed aerosol surface area dominates at rapid oxidation rates and relatively low seed aerosol surface area.

5. Conclusion

This work applies a computational model to simulate the dynamics of vapors and particles in an environmental chamber in which a VOC is undergoing oxidation to generate SOA. Here, we explore numerically the competitive processes involving vapors, particles, and the chamber walls in such a system. In order to avoid technicalities of actual gas-phase kinetics, we have utilized the canonical reaction system of A → B → C → D, in which each reaction product is characterized by decreasing volatility from its predecessor. Several key parameters emerge as strongly influencing the rate of generation of SOA; these include the accommodation coefficients of vapor species on growing particles and the wall, α_p and α_w, respectively, and the equilibrium solubility of vapors in the wall itself, C_w. We have also assessed the effect of particle–particle coagulation on particle dynamics and SOA formation. The challenge now remains to simulate chamber dynamics in actual VOC systems with explicit oxidation kinetics and array of reaction products.

Funding

SMC acknowledges support by a U.S. National Science Foundation Graduate Research Fellowship under Grant No. 1745301. This work was also supported by U.S. National Science Foundation grant AGS-1523500.

References

Abramson, E., Imre, D., Beranek, J., Wilson, J., and Zelenyuk, A. (2013). Experimental Determination of Chemical Diffusion within Secondary Organic Aerosol Particles. *Phys. Chem. Chem. Phys.*, 15:2983–2991. doi:10.1039/c2cp44013j.

Adams, P. J., and Seinfeld, J. H. (2002). Predicting Global Aerosol Size Distributions in General Circulation Models. *J. Geophys. Res.*, 107:4370, doi: 10.1029/2001JD001010. doi:10.1029/2001JD001010.

Bian, Q., May, A. A., Kreidenweis, S. M., and Pierce, J. R. (2015). Investigation of Particle and Vapor Wall-Loss Effects on Controlled Wood-Smoke Smog-Chamber Experiments. *Atmos. Chem. Phys.*, 15:11027–11045. doi:10.5194/acp-15-11027-2015.

Bian, Q., Jathar, S. H., Kodros, J. K., Barsanti, K. C., Hatch, L. E., May, A. A., Kreidenweis, S. M., and Pierce, J. R. (2017). Secondary Organic Aerosol Formation in Biomass-Burning Plumes: Theoretical Analysis of Lab Studies and Ambient Plumes. *Atmos. Chem. Phys.*, 17:5459–5475. doi:10.5194/acp-17-5459-2017.

Crump, J. G., and Seinfeld, J. H. (1981). Turbulent Deposition and Gravitational Sedimentation of an Aerosol in a Vessel of Arbitrary Shape. *J. Aerosol Sci.*, 12:405–415. doi:10.1016/0021-8502(81)90036-7.

Hildebrandt, L., Donahue, D. M., and Pandis, S. N. (2009). High Formation of Secondary Organic Aerosol from the Photo-oxidation of Toluene. *Atmos. Chem. Phys.*, 9:2973–2986. doi:10.5194/acp-9-2973-2009.

Julin, J., Winkler, P. M., Donahue, N. M., Wagner, P. E., and Riipinen, I. (2014). Near-Unity Mass Accommodation Coefficient of Organic Molecules of Varying Structure. *Environ. Sci. Technol.*, 48:12083–12089. doi:10.1021/es501816h.

Kolb, C. E., Cox, R. A., Abbatt, J. P. D., Ammann, M., Davis, E. J., Donaldson, D. J., Garrett, B. C., George, C., Griffiths, P. T., Hanson, D. R., Kulmala, M., McFiggans, G., Pöschl, U., Riipinen, I., Rossi, M. J., Rudich, Y., Wagner, P. E., Winkler, P. M., Worsnop, D. R., and O'Dowd, C. D. (2010). An Overview of Current Issues in the Uptake of Atmospheric Trace Gases by Aerosols and Clouds. *Atmos. Chem. Phys.*, 10:10561–10605. doi:10.5194/acp-10-10561-2010.

Krechmer, J. E., Pagonis, D., Ziemann, P. J., and Jimenez, J. L. (2016). Quantification of Gas-Wall Partitioning in Teflon Environmental Chambers Using Rapid Bursts of Low-Volatility Oxidized Species. *Environ. Sci. Technol.*, 50:5757–5765. doi:10.1021/acs.est.6b00606.

Loza, C. L., Chan, A. W. H., Galloway, M. M., Kuetsch, F. N., Flagan, R. C., and Seinfeld, J. H. (2010). Characterization of Vapor Wall Loss in Laboratory Chambers. *Environ. Sci. Technol.*, 44:5074–5078. doi:10.1021/es100727v.

Mai, H., Shiraiwa, M., Flagan, R. C., and Seinfeld, J. H. (2015). Under What Conditions Can Equilibrium Gas-Particle Partitioning Be Expected to Hold in the Atmosphere? *Environ. Sci. Technol.*, 49:11485–11491. doi:10.1021/acs.est.5b02587.

Matsunaga, A., and Ziemann, P. J. (2010). Gas-Wall Partitioning of Organic Compounds in a Teflon Film Chamber and Potential Effects on Reaction Product and Aerosol Yield Measurements. *Aerosol Sci. Technol.*, 44:881–892. doi:10.1080/02786826.2010.501044.

McMurry, P. H., and Grosjean, D. (1985). Gas and Aerosol Losses in Teflon Film Smog Chambers. *Environ. Sci. Technol.*, 19:1176–1182. doi:10.1021/es00142a006.

McMurry, P. H., and Rader, D. J. (1985). Aerosol Wall Losses in Electrically Charged Chambers. *Aerosol Sci. Technol.*, 4:249–268. https://doi.org/10.1080/02786828508959054.

McVay, R. C., Cappa, C. D., and Seinfeld, J. H. (2014). Vapor-Wall Deposition in Chambers: Theoretical Considerations. *Environ. Sci. Technol.*, 48:10251–10258. doi:10.1021/es502170j.

Meng, Z., Dabdub, D., and Seinfeld, J. H. (1998). Size-Resolved and Chemically Resolved Model of Atmospheric Aerosol Dynamics. *J. Geophys. Res.*, 103:3419–3435. doi:10.1029/97JD02796.

Nah, T., McVay, R. C., Zhang, X., Boyd, C. M., Seinfeld, J. H., and Ng, N. L. (2016). Influence of Seed Aerosol Surface Area and Oxidation Rate on Vapor Wall Deposition and SOA Mass Yields: A Case Study with α-pinene Ozonolysis. *Atmos. Chem. Phys.*, 16:9361–9372. doi:10.5194/acp-16-9361-2016.

Nah, T., McVay, R. C., Pierce, J. R., Seinfeld, J. H., and Ng, N. L. (2017). Constraining Uncertainties in Particle-Wall Deposition Correction During SOA Formation in Chamber Experiments. *Atmos. Chem. Phys.*, 17:2297–2310. doi:10.5194/acp-17-2297-2017.

Pierce, J. R., Engelhart, G. J., Hildebrandt, L., Weitkamp, E. A., Pathak, R. K., Donahue, N. M., Robinson, A. L., Adams, P. J., and Pandis, S. N. (2008). Constraining Particle Evolution from

Wall Losses, Coagulation, and Condensation-Evaporation in Smog Chamber Experiments: Optimal Estimation Based on Size Distribution Measurements. *Aerosol Sci. Technol.*, 42:1001–1015. doi:10.1080/02786820802389251.

Pierce, J. R., and Adams, P. J. (2009). A Computationally Efficient Aerosol Nucleation/Condensation Method: Pseudo-Steady-State Sulfuric Acid. *Aerosol Sci. Technol.*, 43:216–226. doi:10.1080/02786820802587896.

Pilinis, C. (1990). Derivation and Numerical Solution of the Species Mass Distribution Equations for Multicomponent Particulate Systems. *Atmos. Environ.*, 24:1923–1928. doi:10.1016/0960-1686(90)90525-R.

Russell, L. M., and Seinfeld, J. H. (1998). Size- and Composition-Resolved Externally Mixed Aerosol Model. *Aerosol Sci. Technol.*, 28:403–416. doi:10.1080/02786829808965534.

Saleh, R., Donahue, N. M., and Robinson, A. L. (2013). Time Scales for Gas-Particle Partitioning Equilibration of Secondary Organic Aerosol Formed from Alpha-Pinene Ozonolysis. *Environ. Sci. Technol.*, 47:5588–5594. doi:10.1021/es400078d.

Schwantes, R. H., McVay, R. C., Zhang, X., Coggon, M. M., Lignell, H., Flagan, R. C., Wennberg, P. O., and Seinfeld, J. H. (2017). Science of the Environmental Chamber, in *Advances in Atmospheric Chemistry*, Volume I, World Scientific, Singapore, pp. 1–93.

Seinfeld, J. H., and Pandis, S. N. (2016). *Atmospheric Chemistry and Physics: from Air Pollution to Climate Change* 3rd Ed., Wiley, Hoboken, N.J.

Shiraiwa, M., Seinfeld, J. H. (2012). Equilibration Time Scale of Atmospheric Secondary Organic Aerosol Partitioning. *Geophys. Res. Lett.*, 39:L24801. doi:10.1029/2012GL054008.

Shiraiwa, M., Zuend, A., Bertram, A. K., and Seinfeld, J. H. (2013). Gas-Particle Partitioning of Atmospheric Aerosols: Interplay of Physical State, Non-ideal Mixing and Morphology. *Phys. Chem. Chem. Phys.*, 15:11441–11453. doi:10.1039/c3cp51595h.

Tian, J., Brem, B. T., West, M., Bond, T. C., Rood, M. J., and Riemer, N. (2017). Simulating Aerosol Chamber Experiments with the Particle-Resolved Aerosol Model Part MC. *Aerosol Sci. Technol.*, 51:856–867. doi:10.1080/02786826.2017.1311988.

Trump, E. R., Epstein, S. A., Riipinen, I., and Donahue, N. M. (2016). Wall Effects in Smog Chamber Experiments: A Model Study. *Aerosol Sci. Technol.*, 50:1180–1200. doi:10.1080/02786826.2016.1232858.

Vaden, T. D., Song, C., Zaveri, R. A., Imre, D., and Zeleyuk A. (2010). Morphology of Mixed Primary and Secondary Organic Particles and the Adsorption of Spectator Organic Gases During Aerosol Formation. *Proc. Natl. Acad. Sci. USA.*, 107:6658–6663. doi:10.1073/pnas.0911206107.

Vaden, T. D., Imre, D., Balanek, J., Shrivastava, M., and Zeleyuk, A. (2011). Evaporation Kinetics and Phase of Laboratory and Ambient Secondary Organic Aerosol. *Proc. Natl. Acad. Sci. USA.*, 108:2190–2195. doi:10.1073/pnas.1013391108.

Virtanen, A., Joutsensaari, J., Koop, T., Kannosto, J., Yli-Pirilä, P., Leskinen, J., Makela, J. M., Holopainen, K. J., Pöschl, U., Kulmala, M., Worsnop, D. R., and Laaksonen, A. (2010a). An Amorphous Solid State of Biogenic Secondary Organic Aerosol Particles. *Nature*, 467:824–827. doi:10.1038/nature09455.

Virtanen, A., Kannosto, J., Kuuluvainen, H., Arffman, A., Joutsensaari, J., Saukko, E., Hao, L., Yli-Pirilä, P., Tiitta, P., Holopainen, K. J., Keskinen, J., Worsnop, D. R., Smith, J. N., and Laaksonen, A. (2010b). Bounce Behavior of Freshly Nucleated Biogenic Secondary Organic Aerosol Particles. *Atmos. Chem. Phys.*, 11:8759–8766. doi:10.5194/acp-11-8759-2011.

Ye, P., Ding, X., Hakala, J., Hofbauer, V., Robinson, E. S., and Donahue, N. M. (2016). Vapor Wall Loss of Semi-volatile Organic Compounds in Teflon Chamber. *Aerosol Sci. Technol.*, 50:822–834. doi:10.1080/02786826.2016.1195905.

Yeh, G. K., and Ziemann, P. J. (2015). Gas-Wall Partitioning of Oxygenated Organic Compounds: Measurements, Structure-Activity Relationships and Correlation with Gas Chromatographic Retention Factor. *Aerosol Sci. Technol.*, 49:726–737. doi:10.1080/02786826.2015.1068427.

Zaveri, R. A., Easter, R. C., Shilling, J. E., and Seinfeld, J. H. (2014). Modeling Kinetic Partitioning of Secondary Organic Aerosol and Size Distribution Dynamics: Representing Effects of Volatility, Phase State, and Particle-Phase Reaction. *Atmos. Chem. Phys.*, 14:5153–5181. doi:10.5194/acp-14-5153-2014.

Zhang, X., Pandis, S. N., and Seinfeld, J. H. (2012). Diffusion-Limited versus Quasi-Equilibrium Aerosol Growth. *Aerosol Sci. Technol.*, 46:874–885. doi:10.1080/02786826.2012.679344.

Zhang, X., Cappa, C. D., Jathar, S. H., McVay, R. C., Ensberg, J. J., Kleeman, M. J., and Seinfeld, J. H. (2014). Influence of Vapor Wall Loss in Laboratory Chambers on Yields of Secondary Organic Aerosol. *Proc. Natl. Acad. Sci. USA.*, 111:5802–5807. doi:10.1073/pnas.1404727111.

Zhang, X., Schwantes, R. H., McVay, R. C., Lignell, H., Coggon, M. M., Flagan, R. C., and Seinfeld, J. H. (2015). Vapor Wall Deposition in Teflon Chambers. *Atmos. Chem. Phys.*, 15:4197–4214. doi:10.5194/acp-15-4197-2015.